



Real-time numerical differentiation of sampled data using adaptive input and state estimation

Shashank Verma, Sneha Sanjeevini, E. Dogan Sumer & Dennis S. Bernstein

To cite this article: Shashank Verma, Sneha Sanjeevini, E. Dogan Sumer & Dennis S. Bernstein (13 Feb 2024): Real-time numerical differentiation of sampled data using adaptive input and state estimation, International Journal of Control, DOI: [10.1080/00207179.2024.2313046](https://doi.org/10.1080/00207179.2024.2313046)

To link to this article: <https://doi.org/10.1080/00207179.2024.2313046>



Published online: 13 Feb 2024.



Submit your article to this journal [↗](#)



Article views: 18



View related articles [↗](#)



View Crossmark data [↗](#)



Real-time numerical differentiation of sampled data using adaptive input and state estimation

Shashank Verma ^a, Sneha Sanjeevini ^a, E. Dogan Sumer ^b and Dennis S. Bernstein ^a

^aDepartment of Aerospace Engineering, University of Michigan, Ann Arbor, MI, USA; ^bFord Motor Company, Dearborn, MI, USA

ABSTRACT

Real-time numerical differentiation plays a crucial role in many digital control algorithms, such as PID control, which requires numerical differentiation to implement derivative action. This paper proposes an algorithm for estimating the numerical derivative of a signal from noisy sampled data measurements. The method uses adaptive input estimation with adaptive state estimation (AIE/ASE), and thus it requires only minimal prior information about the signal and noise statistics. Furthermore, since the estimates of the derivative at step k provided by AIE/ASE depend only on data available up to step k , AIE/ASE is thus implementable in real time. The accuracy of AIE/ASE is compared numerically to several conventional numerical differentiation methods. Finally, AIE/ASE is applied to simulated vehicle position data, generated in the CarSim simulator software.

ARTICLE HISTORY

Received 12 February 2023
Accepted 26 January 2024

KEYWORDS

Numerical differentiation;
Adaptive system; Kalman
filter; Input estimation

1. Introduction

The dual operations of integration and differentiation provide the foundation for much of mathematics. Analytically, differentiation is often considered less complex than integration, as evidenced by the relative difficulty encountered in differentiating versus integrating functions such as $\log(1 + \sin^2 x^3)$. In numerical analysis, integration techniques have been extensively developed in Davis and Rabinowitz (1984), whereas differentiation techniques have been developed more sporadically in Savitzky and Golay (1964), Cullum (1971), and Hamming (1973, pp. 565, 566).

In practice, numerical integration and differentiation techniques are applied to sequences of measurements, that is, discrete-time signals composed of sampled data. Although strictly speaking, integration and differentiation are defined on continuous spaces and not for discrete-time signals, the goal is to compute a discrete-time ‘integral’ or ‘derivative’ estimate that approximates the true integral or derivative of the pre-sampled, analog signal.

In addition to the effect of sampling, numerical integration and differentiation methods must address the effect of sensor noise in sampled data. For numerical integration of sampled data, constant noise in data, that is, bias, leads to a spurious ramp, while stochastic noise leads to random-walk divergence due to the numerical integration of noise present in the data. Mitigation of these effects is of extreme importance in applications such as inertial navigation as shown in Farrell (2008) and Grewel et al. (2020).

Compared to numerical integration, the effect of noise on numerical differentiation is far more severe. This situation is due to the fact that, whereas integration is a bounded operator on a complete inner-product space, differentiation is an

unbounded operator on a dense subspace. Unboundedness implies a lack of continuity, which is manifested as high sensitivity to sensor noise. Consequently, numerical differentiation typically involves assumptions on the smoothness of the signal and spectrum of the noise as considered in Ahn et al. (2006), Jauberteau and Jauberteau (2009), Stickel (2010), Listmann and Zhao (2013), Knowles and Renka (2014), and Haimovich et al. (2022).

Numerical differentiation algorithms are crucial elements of many digital control algorithms. For example, PID control requires numerical differentiation to implement derivative action as presented in Vilanova and Visioli (2012) and Astrom and Hagglund (2006). Flatness-based control is based on a finite number of derivatives as shown in Nieuwstadt et al. (1998) and Mboup et al. (2009). In feedback control applications, real-time implementation of numerical differentiation algorithms is essential. However, the phase shift and latency associated with numerical differentiation can result in performance degradation and even instability. Phase shift arises from filtering, whereas latency arises from noncausal numerical differentiation, that is, numerical differentiation algorithms that require future data. For real-time applications, a noncausal differentiation algorithm that requires data at future time steps can be implemented causally by delaying the computation until the required data are available. For feedback controllers that require an estimate of the *current* derivative, the delayed estimate provided by a noncausal differentiation algorithm may not be a sufficiently accurate estimate of the required derivative.

In practice, analog or digital filters are used to suppress the effect of sensor noise, thereby allowing the use of differencing formulae in the form of inverted ‘V’ filters, which have the required gain and phase lead at low frequencies and roll off at

high frequencies. These techniques assume that the characteristics of the signal and noise are known, thereby allowing the user to tweak the filter parameters. When both the true signal and the noise have characteristics that are unknown and may change over time, filter tuning becomes impossible, significantly increasing the challenge of the problem. The recent work in Van Breugel et al. (2020) articulates these challenges and proposes a Pareto-tradeoff technique for addressing the absence of prior information. Additional techniques include high-gain observer methods, where the observer approximates the dynamics of a differentiator as shown in Dabroom and Khalil (1999). Li et al. (2018) employed a kernel-based deadbeat observer for numerical differentiation, utilising Volterra integral operators. Numerical differentiation based on integration using Jacobi polynomials was introduced in Da-yan Liu and Perruquetti (2011). Yet another approach is to apply sliding-mode algorithms as shown in Levant (2003), Reichhartinger and Spurgeon (2018), López-Caamal and Moreno (2019), Mojallizadeh et al. (2021), Alwi and Edwards (2013), and Levant (1998). Ibrir and Diop (2004) presented a method involving a simplified linear optimisation problem to deduce a continuous spline signal, aiding in the estimation of the derivative of sampled data. Additionally, Polyakov et al. (2014) analysed a homogeneous differentiator based on the implicit Lyapunov function method.

Another approach to numerical differentiation is to apply state estimation with integrator dynamics, where the state estimate includes an estimate of the derivative of the measurement as shown in Kalata (1984) and Bogler (1987). This approach has been widely used for target and vehicle tracking in Jia et al. (2008), Khaloozadeh and Karsaz (2009), Lee and Tahk (1999), and Rana et al. (2020). As an extension of state estimation, the present paper applies input estimation to numerical differentiation, where the goal is to estimate the input as well as the state. Input and state estimation methods are discussed in Gillijns and De Moor (2007), Orjuela et al. (2009), Fang et al. (2011), Yong et al. (2016), Hsieh (2017), Naderi and Khorasani (2019), and Alenezi et al. (2021).

The present paper is motivated by the situation where minimal prior information about the signal and noise is available. This case arises when the spectrum of the signal changes slowly or abruptly in an unknown way, and when the noise characteristics vary due to changes in the environment, such as weather. With this motivation, adaptive input estimation (AIE) was applied to target tracking in Ansari and Bernstein (2019), where it was used to estimate vehicle acceleration using position data. In particular, the approach of Ansari and Bernstein (2019) is based on retrospective cost input estimation (RCIE), where recursive least squares (RLS) is used to update the coefficients of the estimation subsystem. The error metric used for adaptation is the residual (innovations) of the state estimation algorithm, that is, the Kalman filter. This technique requires specification of the covariances of the process noise, input-estimation error, and sensor noise. The present paper extends the approach of Ansari and Bernstein (2019) by replacing the Kalman filter with an adaptive Kalman filter in which the input-estimation-error covariance and the sensor-noise covariance are updated online. Adaptive extensions of the Kalman filter to the case where the variance of the disturbance is unknown are considered in Yaesh and Shaked (2008), Shi et al. (2009), Moghe

et al. (2019), and Zhang et al. (2020). Adaptive Kalman filters based on the residual for integrating INS/GPS systems are discussed in Mohamed and Schwarz (1999), Hide et al. (2003), and Almagbile et al. (2010). Several approaches to adaptive filtering, such as Bayesian, maximum likelihood, correlation, and covariance matching, are studied in Mehra (1972). A related algorithm involving a covariance constraint is developed in Mook and Junkins (1988). The adaptive Kalman filter used in the present paper as part of adaptive input estimation with adaptive state estimation (AIE/ASE) is based on a search over the range of input-estimation error covariance. This technique has proven to be easy to implement and effective in the presence of unknown signal and noise characteristics. The main contribution of the present paper is a numerical investigation of the accuracy of AIE combined with the proposed adaptive state estimation (ASE) in the presence of noise with unknown properties. The accuracy of AIE/ASE is compared to the backward-difference differentiation, Savitzky-Golay differentiation (Mboup et al., 2009; Savitzky & Golay, 1964; Schafer, 2011; Staggs, 2005), and numerical differentiation based on high-gain observers (Dabroom & Khalil, 1999).

The present paper represents a substantial extension of preliminary results presented in Verma et al. (2022). In particular, the algorithms presented in the present paper extend the adaptive estimation component of the approach of Verma et al. (2022) in Section 5, and the accuracy of these algorithms is more extensively evaluated and compared to prior methods in Section 6.

The contents of the paper are as follows. In Section 2, we identify the challenges that arise from implementing numerical differentiation algorithms in real time. These challenges are primarily due to the delay in the availability of the estimated derivative, which results from computation time and non-causality. This section also defines an error metric for comparing the accuracy of the algorithms considered in this paper. Section 3 summarises three baseline numerical differentiation algorithms and identifies their limitations, which motivates the proposed algorithm. Section 4 summarises the adaptive input estimation algorithm. Section 5 provides the paper's main contribution, namely, adaptive input estimation with adaptive state estimation (AIE/ASE), along with its two other variations. Section 6 applies three variations of AIE using harmonic signals with various noise levels. Finally, Section 7 applies the variations of AIE to simulated vehicle position data generated by CarSim.

2. Problem statement and error metric

This section presents the problem statement and error metric used to assess the accuracy of the algorithms presented in this paper. The error metric is specifically chosen to reflect the implications of real-time implementation.

2.1 Problem statement

Let y be a continuous-time signal with q th derivative $y^{(q)}$. We assume that the sampled values $y_k \triangleq y(kT_s)$ are available, where T_s is the sample time. The goal is to use the sampled values y_k to obtain an estimate $\hat{y}_k^{(q)}$ of $y_k^{(q)} \triangleq y^{(q)}(kT_s)$ in the presence

of measurement noise with unknown properties. This paper focuses on the cases $q = 1$ and $q = 2$.

2.2 Real-time implementation and error metric

The time T_c required for computation in numerical differentiation invariably results in a delay of δ time steps before the estimated derivative becomes available. In this paper, we assume that $T_c \leq T_s$, and thus the delay due to computation time is $\delta = 1$.

This paper considers both causal and noncausal differentiation methods. To estimate the derivative at the current step, causal differentiation does not require future data; in contrast, noncausal differentiation utilises future data. For real-time implementation, causal differentiation entails a delay of $\delta = 1$ step due to the computation time T_c , whereas noncausal differentiation entails a delay of $\delta \geq 2$ steps. For the case $\delta = 1$, Figure 1 shows that the estimate $\hat{y}_k^{(q)}$ of $y_k^{(q)}$ is not available until step $k + 1$. To quantify the accuracy of each numerical differentiation algorithm, for all $k \geq \delta$, we define the relative root-mean-square error (RMSE) of the estimate of the q th derivative as

$$\rho_k^{(q)} \triangleq \sqrt{\frac{\sum_{i=\delta}^k (y_i^{(q)} - \hat{y}_{i-\delta}^{(q)})^2}{\sum_{i=\delta}^k (y_{i-\delta}^{(q)})^2}}. \quad (1)$$

Note that the numerator of (1) accounts for the effect of the delay δ . For real-time implementation, the relevant error metric depends on the difference between the true current derivative and the currently available estimate of the past derivative, as can be seen in the numerator of (1). When the derivative estimates are exact, (1) determines an RMSE value that can be viewed as the *delay floor* for the q th derivative, that is, the error due solely to the fact that a noncausal differentiation algorithm must be implemented with a suitable delay. Note that the delay floor depends on δ and is nonnegative.

The *true* values of $y_k^{(q)}$ are the sampled values of $y^{(q)}$ in the absence of sensor noise. Of course, the true values of $y_k^{(q)}$ are

unknown in practice and thus cannot be used as an online error criterion. However, these values are used in (1), which is computable in simulation for comparing the accuracy of the numerical differentiation algorithms.

3. Comparison and limitations of baseline algorithms

This section summarises three algorithms for numerically differentiating sampled data. These algorithms provide a baseline for evaluating the accuracy of the adaptive input and state estimation algorithms described in Section 5.

3.1 Backward-difference (BD) differentiation

As define in Astrom and Hagglund (2006), let \mathbf{q}^{-1} denote the backward-shift operator. Then the *backward-difference single differentiator* is given by

$$G_{sd}(\mathbf{q}^{-1}) \triangleq \frac{1 - \mathbf{q}^{-1}}{T_s}, \quad (2)$$

and the *backward-difference double differentiator* is given by

$$G_{dd}(\mathbf{q}^{-1}) \triangleq \frac{(1 - \mathbf{q}^{-1})^2}{T_s^2}. \quad (3)$$

3.2 Savitzky–Golay (SG) differentiation

As shown in Savitzky and Golay (1964), Schafer (2011), and Staggs (2005), in SG differentiation at each step k , a polynomial

$$P_k(s) = \sum_{i=0}^{p_d} a_{i,k} s^i \quad (4)$$

of degree p_d is fit over a sliding data window of size $2\ell + 1$ centred at step k , where $\ell \geq 1$. At each step k , this leads to the

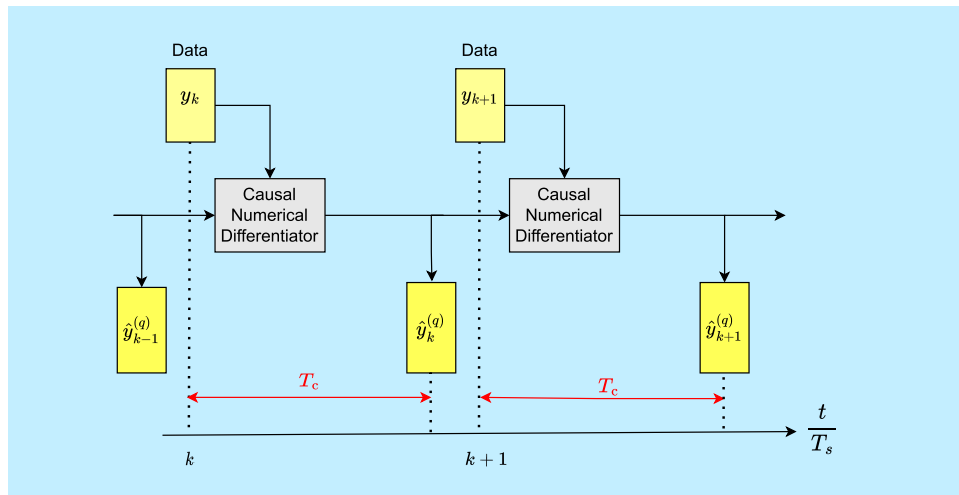


Figure 1. Timing diagram for causal numerical differentiation. The causal numerical differentiator uses data obtained at step k to estimate the derivative of the signal y . Because of the computation time T_c , the estimate $\hat{y}_k^{(q)}$ of $y_k^{(q)}$ is not available until step $k + 1$. In this case, the delay is $\delta = 1$ step. For noncausal differentiation, $\delta \geq 2$.

least-squares problem

$$\min \|\mathcal{Y}_k - \mathcal{A}_k \mathcal{X}_k\|, \quad (5)$$

where

$$\mathcal{Y}_k \triangleq \begin{bmatrix} y_{k-\ell} \\ \vdots \\ y_{k+\ell} \end{bmatrix}, \quad \mathcal{X}_k \triangleq \begin{bmatrix} a_{0,k} \\ \vdots \\ a_{p_d,k} \end{bmatrix}, \quad (6)$$

$$\mathcal{A}_k \triangleq \begin{bmatrix} 1 & (k-\ell)T_s & \cdots & ((k-\ell)T_s)^{p_d} \\ \vdots & \vdots & \ddots & \vdots \\ 1 & (k+\ell)T_s & \cdots & ((k+\ell)T_s)^{p_d} \end{bmatrix}. \quad (7)$$

Solving (5) with $q \leq p_d \leq 2\ell$ yields

$$\hat{\mathcal{X}}_k = \begin{bmatrix} \hat{a}_{0,k} \\ \vdots \\ \hat{a}_{p_d,k} \end{bmatrix}. \quad (8)$$

Differentiating (4) q times with respect to s , setting $s = kT_s$, and replacing the coefficients of P_k in (4) with the components of $\hat{\mathcal{X}}_k$, the estimate $\hat{y}_k^{(q)}$ of $y_k^{(q)}$ is given by

$$\hat{y}_k^{(q)} = \sum_{i=q}^{p_d} Q_{i,q} \hat{a}_{i,k} (kT_s)^{i-q}, \quad (9)$$

where, for all $i = q, \dots, p_d$,

$$Q_{i,q} \triangleq \prod_{j=1}^q (i-j+1). \quad (10)$$

3.3 High-gain-observer (HGO) differentiation

A state space model for the r th-order continuous-time HGO in Dabroom and Khalil (1999) is given by

$$\dot{\hat{x}} = A_{co} \hat{x} + B_{co} y, \quad \hat{y} = C_o \hat{x}, \quad (11)$$

$$A_{co} \triangleq \begin{bmatrix} 0_{(r-1) \times 1} & I_{r-1} \\ 0 & 0_{1 \times (r-1)} \end{bmatrix} - H \begin{bmatrix} 1 & 0_{1 \times (r-1)} \end{bmatrix}, \quad (12)$$

$$C_o \triangleq \begin{bmatrix} 0_{(r-1) \times 1} & I_{r-1} \end{bmatrix}, \quad (13)$$

$$B_{co} = H \triangleq \begin{bmatrix} \alpha_1 & \alpha_2 & \cdots & \alpha_r \\ \varepsilon & \varepsilon^2 & \cdots & \varepsilon^r \end{bmatrix}^T, \quad (14)$$

where $\varepsilon > 0$ and $\alpha_1, \dots, \alpha_r$ are constants chosen such that the polynomial

$$p(s) \triangleq s^r + \alpha_1 s^{r-1} + \cdots + \alpha_{r-1} s + \alpha_r \quad (15)$$

is Hurwitz. The transfer function from y to \hat{y} is given by

$$G(s) = C_o (sI - A_{co})^{-1} H = D_G^{-1}(s) N_G(s), \quad (16)$$

where

$$D_G(s) \triangleq \varepsilon^r s^r + \alpha_1 \varepsilon^{r-1} s^{r-1} + \cdots + \alpha_{r-1} \varepsilon s + \alpha_r, \quad (17)$$

$$N_G(s) \triangleq \begin{bmatrix} \alpha_2 \varepsilon^{r-2} s^{r-1} + \cdots + \alpha_{r-1} \varepsilon s^2 + \alpha_r s \\ \alpha_3 \varepsilon^{r-3} s^{r-1} + \cdots + \alpha_{r-1} \varepsilon s^3 + \alpha_r s^2 \\ \vdots \\ \alpha_{r-1} \varepsilon s^{r-1} + \alpha_r s^{r-2} \\ \alpha_r s^{r-1} \end{bmatrix}. \quad (18)$$

Since

$$\lim_{\varepsilon \rightarrow 0} G(s) = \begin{bmatrix} s & s^2 & \cdots & s^{r-1} \end{bmatrix}^T, \quad (19)$$

it follows that, for all $i = 1, \dots, r-1$, the i th component of \hat{y} is an approximation of $y^{(i)}$. Applying the bilinear transformation to (11) yields the discrete-time observer

$$\hat{x}_{k+1} = A_{do} \hat{x}_k + B_{do} y_k, \quad \hat{y}_k = C_o \hat{x}_k, \quad (20)$$

where

$$A_{do} \triangleq (I_r - \frac{1}{2} T_s A_{co})^{-1} (I_r + \frac{1}{2} T_s A_{co}), \quad (21)$$

$$B_{do} \triangleq (I_r - \frac{1}{2} T_s A_{co})^{-1} B_{co} T_s. \quad (22)$$

Implementation of (20) provides estimates $\hat{y}_k^{(1)}, \dots, \hat{y}_k^{(r-1)}$ of $y_k^{(1)}, \dots, y_k^{(r-1)}$.

Several noteworthy differences exist among BD, SG, and HGO. First, BD differentiation operates on adjacent pairs of data points, whereas SG differentiation operates on a moving window of data points. Consequently, SG differentiation is potentially more accurate than BD differentiation.

To compare the presented baseline algorithms, we consider numerical differentiation of the continuous-time signal $y(t) = \sin(20t)$, where t is time in seconds. The signal $y(t)$ is sampled with sample time $T_s = 0.01$ sec. The measurements are assumed to be corrupted by noise, and thus the noisy sampled signal is given by $y_k = \sin(0.2k) + Dv_k$, where v_k is standard (zero-mean, unit-variance, Gaussian) white noise. The value of D is chosen to set the desired signal-to-noise ratio (SNR).

For single differentiation with SG, let $\ell = 2$ and $p_d = 3$. For single differentiation with HGO, let HGO/1 denote HGO with $r = 2, \alpha_1 = 2, \alpha_2 = 1$, and $\varepsilon = 0.2$, and let HGO/2 denote HGO/1 with $\varepsilon = 0.2$ replaced by $\varepsilon = 0.7$. Note that $\delta = 1$ for BD and HGO, whereas $\delta = \ell + 1$ for SG with window size $2\ell + 1$. Figure 2 shows the relative RMSE $\rho_{k_f}^{(1)}$ of the estimate of the first derivative for SNR ranging from 20 dB to 60 dB, where $k_f = 2000$ steps.

The comparison between HGO/1 and HGO/2 in Figure 2 shows that the performance of HGO differentiation depends on the noise level, and thus tuning is needed to achieve the best possible performance. When the noise level is unknown, however, this tuning is not possible. Hence, we now consider a differentiation technique that adapts to the actual noise characteristics.

4. Adaptive input estimation

This section summarises adaptive input estimation (AIE), which is a specialisation of retrospective cost input estimation (RCIE) derived in Ansari and Bernstein (2019). This section explains how AIE specialises RCIE to the problem of causal numerical differentiation.

Consider the linear discrete-time system

$$x_{k+1} = Ax_k + Bd_k, \quad (23)$$

$$y_k = Cx_k + D_2 v_k, \quad (24)$$

where $k \geq 0$ is the step, $x_k \in \mathbb{R}^n$ is the state, $d_k \triangleq d(kT_s) \in \mathbb{R}$, $v_k \in \mathbb{R}$ is standard white noise, and $D_2 v_k \in \mathbb{R}$ is the sensor

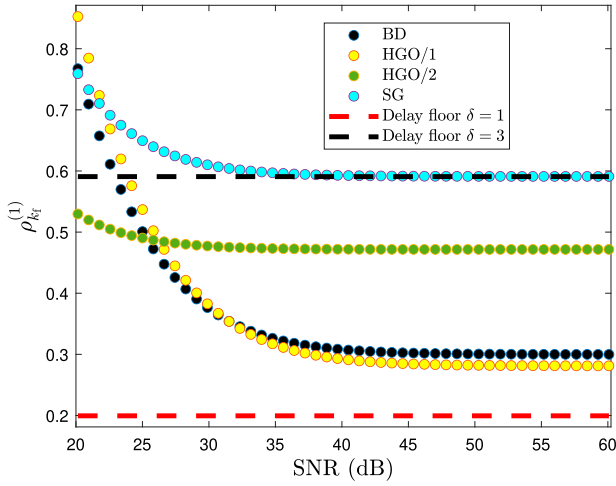


Figure 2. Relative RMSE $\rho_{k_f}^{(1)}$ of the estimate of the first derivative versus SNR, where $k_f = 2000$ steps, for BD, SG, HGO/1, and HGO/2. For the first derivative, the red dashed line denotes the delay floor for $\delta = 1$, and the black dashed line denotes the delay floor for $\delta = 3$.

noise. The matrices $A \in \mathbb{R}^{n \times n}$, $B \in \mathbb{R}^{n \times 1}$, $C \in \mathbb{R}^{1 \times n}$, and $D_2 \in \mathbb{R}$ are assumed to be known. Define the sensor-noise covariance $V_2 \triangleq D_2 D_2^T$. The goal of AIE is to estimate d_k and x_k .

AIE consists of three subsystems, namely, the Kalman filter forecast subsystem, the input-estimation subsystem, and the Kalman filter data-assimilation subsystem. First, consider the Kalman filter forecast step

$$x_{fc,k+1} = Ax_{da,k} + B\hat{d}_k, \quad (25)$$

$$y_{fc,k} = Cx_{fc,k}, \quad (26)$$

$$z_k = y_{fc,k} - y_k, \quad (27)$$

where \hat{d}_k is the estimate of d_k , $x_{da,k} \in \mathbb{R}^n$ is the data-assimilation state, $x_{fc,k} \in \mathbb{R}^n$ is the forecast state, $z_k \in \mathbb{R}$ is the residual, and $x_{fc,0} = 0$.

Next, to obtain \hat{d}_k , the input-estimation subsystem of order n_e is given by

$$\hat{d}_k = \sum_{i=1}^{n_e} P_{i,k} \hat{d}_{k-i} + \sum_{i=0}^{n_e} Q_{i,k} z_{k-i}, \quad (28)$$

where $P_{i,k} \in \mathbb{R}$ and $Q_{i,k} \in \mathbb{R}$ are time-varying coefficients. Note that (28) represents an exactly proper transfer function. AIE minimises z_k by using recursive least squares (RLS) to update $P_{i,k}$ and $Q_{i,k}$ as shown below. The subsystem (28) can be reformulated as

$$\hat{d}_k = \Phi_k \theta_k, \quad (29)$$

where the regressor matrix Φ_k is defined by

$$\Phi_k \triangleq \begin{bmatrix} \hat{d}_{k-1} & \cdots & \hat{d}_{k-n_e} & z_k & \cdots & z_{k-n_e} \end{bmatrix} \in \mathbb{R}^{1 \times l_\theta}, \quad (30)$$

the coefficient vector θ_k is defined by

$$\theta_k \triangleq [P_{1,k} \quad \cdots \quad P_{n_e,k} \quad Q_{0,k} \quad \cdots \quad Q_{n_e,k}]^T \in \mathbb{R}^{l_\theta}, \quad (31)$$

and $l_\theta \triangleq 2n_e + 1$. In terms of the backward-shift operator \mathbf{q}^{-1} , (28) can be written as

$$\hat{d}_k = G_{\hat{d}_k}(\mathbf{q}^{-1})z_k, \quad (32)$$

where

$$G_{\hat{d}_k} \triangleq D_{\hat{d}_k}^{-1} N_{\hat{d}_k}, \quad (33)$$

$$D_{\hat{d}_k}(\mathbf{q}^{-1}) \triangleq I_{l_d} - P_{1,k}\mathbf{q}^{-1} - \cdots - P_{n_e,k}\mathbf{q}^{-n_e}, \quad (34)$$

$$N_{\hat{d}_k}(\mathbf{q}^{-1}) \triangleq Q_{0,k} + Q_{1,k}\mathbf{q}^{-1} + \cdots + Q_{n_e,k}\mathbf{q}^{-n_e}. \quad (35)$$

To update the coefficient vector θ_k , we define the filtered signals

$$\Phi_{f,k} \triangleq G_{f,k}(\mathbf{q}^{-1})\Phi_k, \quad \hat{d}_{f,k} \triangleq G_{f,k}(\mathbf{q}^{-1})\hat{d}_k, \quad (36)$$

where, for all $k \geq 0$,

$$G_{f,k}(\mathbf{q}^{-1}) = \sum_{i=1}^{n_f} \mathbf{q}^{-i} H_{i,k}, \quad (37)$$

$$H_{i,k} \triangleq \begin{cases} CB, & k \geq i = 1, \\ C\bar{A}_{k-1} \cdots \bar{A}_{k-(i-1)}B, & k \geq i \geq 2, \\ 0, & i > k, \end{cases} \quad (38)$$

and $\bar{A}_k \triangleq A(I + K_{da,k}C)$, where $K_{da,k}$ is the Kalman filter gain given by (44) below.

Furthermore, define the *retrospective variable*

$$z_{r,k}(\hat{\theta}) \triangleq z_k - (\hat{d}_{f,k} - \Phi_{f,k}\hat{\theta}), \quad (39)$$

where the coefficient vector $\hat{\theta} \in \mathbb{R}^{l_\theta}$ denotes a variable for optimisation, and define the retrospective cost function

$$\mathcal{J}_k(\hat{\theta}) \triangleq \sum_{i=0}^k [R_z z_{r,i}^2(\hat{\theta}) + R_d (\Phi_i \hat{\theta})^2] + (\hat{\theta} - \theta_0)^T R_\theta (\hat{\theta} - \theta_0), \quad (40)$$

where $R_z \in (0, \infty)$, $R_d \in (0, \infty)$, and $R_\theta \in \mathbb{R}^{l_\theta \times l_\theta}$ is positive definite. Then, for all $k \geq 0$, the unique global minimiser θ_{k+1} of (40) is given by the RLS update as shown in Islam and Bernstein (2019)

$$P_{k+1} = P_k - P_k \tilde{\Phi}_k^T \Gamma_k \tilde{\Phi}_k P_k, \quad (41)$$

$$\theta_{k+1} = \theta_k - P_k \tilde{\Phi}_k^T \Gamma_k (\tilde{z}_k + \tilde{\Phi}_k \theta_k), \quad (42)$$

where

$$P_0 \triangleq R_\theta^{-1}, \quad \Gamma_k \triangleq (\tilde{R}^{-1} + \tilde{\Phi}_k P_k \tilde{\Phi}_k^T)^{-1}, \quad \tilde{\Phi}_k \triangleq \begin{bmatrix} \Phi_{f,k} \\ \Phi_k \end{bmatrix},$$

$$\tilde{z}_k \triangleq \begin{bmatrix} z_k - \hat{d}_{f,k} \\ 0 \end{bmatrix}, \quad \tilde{R} \triangleq \begin{bmatrix} R_z & 0 \\ 0 & R_d \end{bmatrix}.$$

Using the updated coefficient vector given by (42), the estimated input at step $k+1$ is given by replacing k by $k+1$ in (29). We choose $\theta_0 = 0$, and thus $\hat{d}_0 = 0$. Implementation of AIE requires that the user specify the orders n_e and n_f , as well as the weightings R_z , R_d , and R_θ . These parameters are specified for each example in the paper.

4.1 State estimation

The forecast variable $x_{fc,k}$ given by (25) is used to obtain the estimate $x_{da,k}$ of x_k given by the Kalman filter data-assimilation step

$$x_{da,k} = x_{fc,k} + K_{da,k}z_k, \quad (43)$$

where the state estimator gain $K_{da,k} \in \mathbb{R}^n$, the data-assimilation error covariance $P_{da,k} \in \mathbb{R}^{n \times n}$, and the forecast error covariance $P_{f,k+1} \in \mathbb{R}^{n \times n}$ are given by

$$K_{da,k} = -P_{f,k}C^T(CP_{f,k}C^T + V_{2,k})^{-1}, \quad (44)$$

$$P_{da,k} = (I_n + K_{da,k}C)P_{f,k}, \quad (45)$$

$$P_{f,k+1} = AP_{da,k}A^T + V_{1,k}, \quad (46)$$

where $P_{f,0} = 0$ and $V_{1,k} \triangleq B\text{var}(d_k - \hat{d}_k)B^T + \text{Acov}(x_k - x_{da,k}, d_k - \hat{d}_k)B^T + B\text{cov}(d_k - \hat{d}_k, x_k - x_{da,k})A^T$.

4.2 Application of AIE to numerical differentiation

To apply AIE to causal numerical differentiation, (23) and (24) are used to model a discrete-time integrator. AIE then yields an estimate \hat{d}_k of the derivative of the sampled output y_k . For single discrete-time differentiation, $A = 1$, $B = T_s$, and $C = 1$, whereas, for double discrete-time differentiation,

$$A = \begin{bmatrix} 1 & T_s \\ 0 & 1 \end{bmatrix}, \quad B = \begin{bmatrix} \frac{1}{2}T_s^2 \\ T_s \end{bmatrix}, \quad C = [1 \quad 0]. \quad (47)$$

Table 1. Definitions of AIE/NSE, AIE/SSE, and AIE/ASE. Each version of AIE is determined by whether or not $V_{1,k}$ and/or $V_{2,k}$ is adapted in the state-estimation subsystem.

	$V_{1,k}$ Adaptation	$V_{2,k}$ Adaptation
AIE/NSE	No	No
AIE/SSE	Yes	No
AIE/ASE	Yes	Yes

5. Adaptive input and state estimation

In practice, $V_{1,k}$ and $V_{2,k}$ may be unknown in (46) and (44). To address this problem, three versions of AIE are presented. In each version, $V_{1,k}$ and $V_{2,k}$ may or may not be adapted. These versions are summarised in Table 1.

To adapt $V_{1,k}$ and $V_{2,k}$, at each step k we define the computable performance metric

$$J_k(V_1, V_2) \triangleq |\widehat{S}_k - S_k|, \quad (48)$$

where \widehat{S}_k is the sample variance of z_k over $[0, k]$ given by

$$\widehat{S}_k = \frac{1}{k} \sum_{i=0}^k (z_i - \bar{z}_k)^2, \quad (49)$$

$$\bar{z}_k = \frac{1}{k+1} \sum_{i=0}^k z_i, \quad (50)$$

and S_k is the variance of the residual z_k given by the Kalman filter, that is,

$$S_k \triangleq C(AP_{da,k-1}A^T + V_1)C^T + V_2. \quad (51)$$

Note that (48) is the difference between the theoretical and empirical variances of z_k , which provides an indirect measure of the accuracy of V_1 and V_2 .

5.1 AIE with non-adaptive state estimation (AIE/NSE)

In AIE/NSE, V_1 is fixed at a user-chosen constant value, and V_2 is assumed to be known and fixed constant at its true value. AIE/NSE is thus a specialisation of AIE with $V_{1,k} \equiv V_1$ in (46) and $V_{2,k} \equiv V_{2,\text{true}}$ in (44), where $V_{2,\text{true}}$ is the true value of the sensor-noise covariance. A block diagram of AIE/NSE is shown in Figure 3.

5.2 AIE with semi-adaptive state estimation (AIE/SSE)

In AIE/SSE, V_1 is adapted, and V_2 is assumed to be a known and fixed constant at its true value. Let $V_{1,\text{adapt},k}$ denote the adapted value of $V_{1,k}$. AIE/SSE is thus a specialisation of AIE

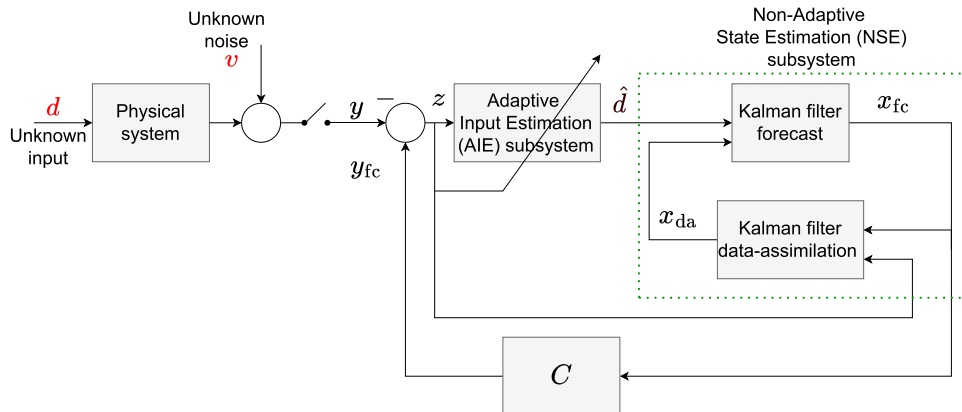


Figure 3. Block diagram of AIE/NSE. The unknown input d is the signal whose estimates are desired, v is sensor noise, and y is the noisy measurement. In this version of AIE, V_1 is fixed at a user-chosen value and V_2 is fixed at its true value. The state estimator is thus not adaptive.

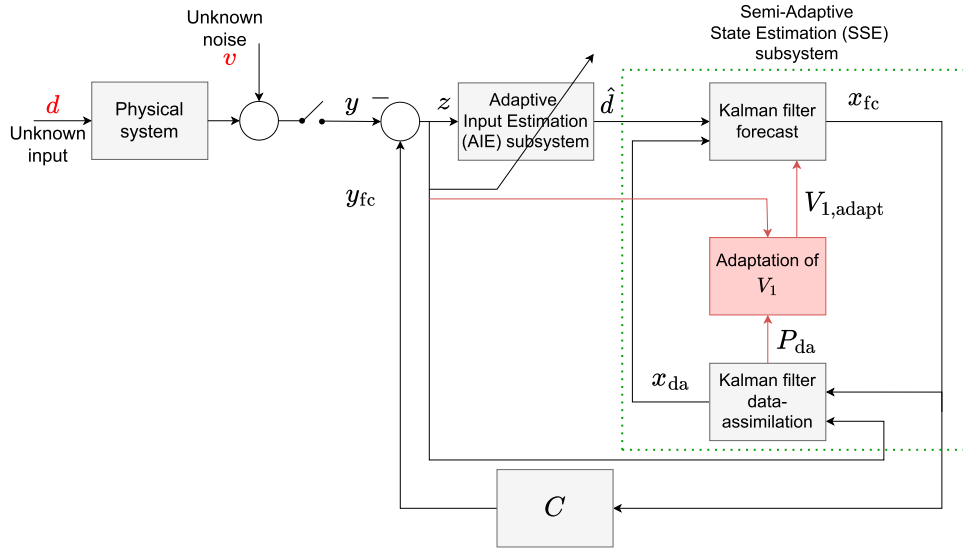


Figure 4. Block diagram of AIE/SSE. In this version of AIE, V_1 is adapted and V_2 is fixed at its true value. The state estimator is thus semi-adaptive.

with $V_{1,k} = V_{1,\text{adapt},k}$ in (46) and $V_{2,k} \equiv V_{2,\text{true}}$ in (44). For all $k \geq 0$, we assume that $V_{1,\text{adapt},k} \triangleq \eta_k I_n$ and we define $\eta_k \in \mathbb{R}$ as

$$\eta_k \triangleq \arg \min_{\eta \in [\eta_L, \eta_U]} J_k(\eta I_n, V_{2,\text{true}}), \quad (52)$$

where $0 \leq \eta_L \leq \eta_U$. Using (48) and (51) to rewrite (52) yields

$$\eta_k = \arg \min_{\eta \in [\eta_L, \eta_U]} |\hat{S}_k - CAP_{\text{da},k-1}A^T C^T - V_{2,\text{true}} - \eta_k CC^T|. \quad (53)$$

A block diagram of AIE/SSE is shown in Figure 4.

5.3 AIE with adaptive state estimation (AIE/ASE)

In AIE/ASE, both V_1 and V_2 are adapted. Let $V_{1,\text{adapt},k} = \eta_k I_n$, where $\eta_k \geq 0$, and $V_{2,\text{adapt},k}$ denote the adapted values of V_1

and V_2 , respectively. Hence, AIE/ASE can be viewed as a specialised form of AIE, with $V_{1,k} = V_{1,\text{adapt},k}$ in (46) and $V_{2,k} = V_{2,\text{adapt},k}$ in (44). The objective is thus to determine $\eta_k \geq 0$ and $V_{2,\text{adapt},k} \geq 0$ such that J_k in (48) is minimised, that is,

$$(\eta_k, V_{2,\text{adapt},k}) \triangleq \arg \min_{\eta \in [\eta_L, \eta_U], V_2 \geq 0} J_k(\eta I_n, V_2), \quad (54)$$

where $0 \leq \eta_L < \eta_U$.

The following result provides the minimising values of η_k and $V_{2,\text{adapt},k}$.

Proposition 5.1: Consider the optimisation problem (54). Define the function $J_{f,k}: \mathbb{R}^{n \times n} \rightarrow \mathbb{R}$ by

$$J_{f,k}(V_1) \triangleq \hat{S}_k - C(AP_{\text{da},k-1}A^T + V_1)C^T, \quad (55)$$

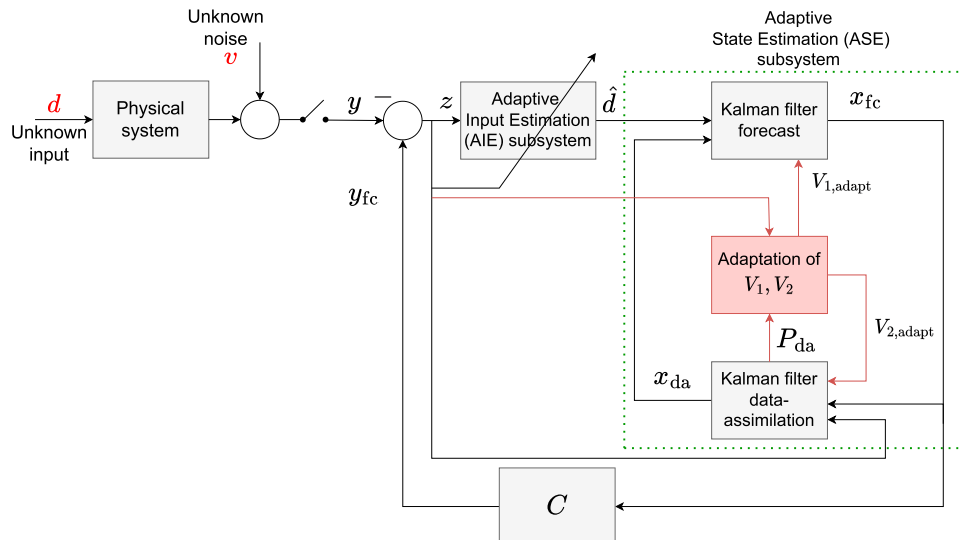


Figure 5. Block diagram of AIE/ASE. In this version of AIE, both V_1 and V_2 are adapted. The state estimator is thus adaptive.

and the set

$$\mathcal{J}_{f,k} \triangleq \{J_{f,k}(\eta I_n) : J_{f,k}(\eta I_n) > 0, \eta_L \leq \eta < \eta_U\} \subseteq (0, \infty). \quad (56)$$

If $\mathcal{J}_{f,k}$ is empty, then a minimiser $(\eta_k, V_{2,\text{adapt},k})$ of (54) is given by

$$\eta_k = \arg \min_{\eta \in [\eta_L, \eta_U]} |J_{f,k}(\eta I_n)|, \quad (57)$$

$$V_{2,\text{adapt},k} = 0, \quad (58)$$

and the minimum value of J_k is

$$J_k(\eta_k I_n, V_{2,\text{adapt},k}) = \widehat{S}_k - CAP_{\text{da},k-1} A^T C^T - \eta_k CC^T.$$

Now, assume that $\mathcal{J}_{f,k}$ is not empty, and let $\widehat{J}_{f,k} \in [\min \mathcal{J}_{f,k}, \max \mathcal{J}_{f,k}]$. Then, a minimiser $(\eta_k, V_{2,\text{adapt},k})$ of (54) is given by

$$\eta_k = \arg \min_{\eta \in [\eta_L, \eta_U]} |J_{f,k}(\eta I_n) - \widehat{J}_{f,k}|, \quad (59)$$

$$V_{2,\text{adapt},k} = J_{f,k}(\eta_k I_n), \quad (60)$$

and the minimum value of J_k is

$$J_k(\eta_k I_n, V_{2,\text{adapt},k}) = 0. \quad (61)$$

Proof: First note that, for all $\eta \in [\eta_L, \eta_U]$ and $V_2 \geq 0$,

$$J_k(\eta I_n, V_2) = |J_{f,k}(\eta I_n) - V_2|. \quad (62)$$

We first consider the case where $\mathcal{J}_{f,k}$ is empty. In this case, for all $\eta \in [\eta_L, \eta_U]$, $J_{f,k}(\eta I_n) \leq 0$. Hence it follows from (62) that (54) is minimised by (57) and (58).

Next, we consider the case where $\mathcal{J}_{f,k}$ is not empty, and thus $\widehat{J}_{f,k} > 0$. With η_k given by (59), it follows that $V_{1,\text{adapt},k} = \eta_k I_n$. Hence, it follows from (59) and (60) that the minimum value of (54) is given by

$$\begin{aligned} J_k(V_{1,\text{adapt},k}, V_{2,\text{adapt},k}) &= |J_{f,k}(V_{1,\text{adapt},k}) - V_{2,\text{adapt},k}| \\ &= |J_{f,k}(\eta_k I_n) - J_{f,k}(\eta_k I_n)| \\ &= 0. \end{aligned}$$

Numerical examples show that

$$\widehat{J}_{f,k} = \frac{1}{2} [\min \mathcal{J}_{f,k} + \max \mathcal{J}_{f,k}] \quad (63)$$

yields a value of η_k that approximately minimises the RMSE (1) of the estimate of the derivative. A block diagram of AIE/ASE is shown in Figure 5. AIE/ASE is summarised by Algorithm 1.

6. Numerical differentiation of two-tone harmonic signal

In this section, a numerical example is given to compare the accuracy of the numerical differentiation algorithms discussed in the previous sections. We consider a two-tone harmonic signal, and we compare the accuracy (relative RMSE) of BD, HGO/1, SG, AIE/NSE, AIE/SSE, and AIE/ASE. For single and double differentiation, the parameters for HGO/1 and SG are given in Section 2.

Algorithm 1 Adaptive Input Estimation/Adaptive State Estimation (AIE/ASE)

```

1: Choose  $n_e \geq 1, n_f \geq 1, R_z, R_d, R_\theta, \eta_L, \eta_U$ ;
2: Set  $x_{fc,0} = 0, P_{f,0} = 0_{n \times n}, K_{\text{da},0} = 0_{n \times 1}, \hat{d}_0 = 0, \theta_{k_n-1} = 0_{l_\theta \times 1}, P_{k_n-1} = R_\theta^{-1} \underline{\gamma}, V_{1,\text{adapt},0} = 0_{n \times n}, V_{2,\text{adapt},0} = 0$ ;
3:  $k_n = \max(n_e, n_f)$ ;  $\bar{R} = \text{blockdiag}(R_z, R_d)$ ;
4: for  $k = 0$  to  $N - 1$  do
  ( $\triangleright$ )Residual
  5:  $y_{fc,k} = Cx_{fc,k}$ ;
  6:  $z_k = y_{fc,k} - y_k$ ;
  ( $\triangleright$ )Adaptive Input Estimation
  7: if  $k < k_n - 1$  do
  8:  $\hat{d}_k = \hat{d}_0$ ;
  9: else do
  10:  $\Phi_k = [\hat{d}_{k-1} \& \dots \& \hat{d}_{k-n_e} \& z_k \& \dots \& z_{k-n_e}]$ ;
  11:  $\hat{d}_k = \Phi_k \theta_k$ ;
  12:  $\bar{A}_{k-1} = A(I_n + K_{\text{da},k-1} C)$ ;
  13: for  $i = 2$  to  $n_f$  do
  14:  $H_{i,k} = C \bar{A}_{k-1} \dots \bar{A}_{k-(i-1)} B$ ;
  15: end for
  16:  $\tilde{H}_k = [CB \& H_{2,k} \& \dots \& H_{n_f,k}]$ ;
  17:  $\Phi_{f,k} = \tilde{H}_k [\Phi_{k-1}^T \& \dots \& \Phi_{k-n_f}^T]^T$ ;
  18:  $\hat{d}_{f,k} = \tilde{H}_k [\hat{d}_{k-1}^T \& \dots \& \hat{d}_{k-n_f}^T]^T$ ;
  19:  $\tilde{\Phi}_k = [\Phi_{f,k}^T \& \Phi_k^T]^T$ ;
  20:  $\tilde{z}_k = [(z_k - \hat{d}_{f,k})^T \& 0]^T$ ;
  21:  $\Gamma_k = (\bar{R}^{-1} + \tilde{\Phi}_k P_k \tilde{\Phi}_k^T)^{-1}$ ;
  22:  $P_{k+1} = P_k - P_k \tilde{\Phi}_k^T \Gamma_k \tilde{\Phi}_k P_k$ ;
  23:  $\theta_{k+1} = \theta_k - P_k \tilde{\Phi}_k^T \Gamma_k (\tilde{z}_k + \tilde{\Phi}_k \theta_k)$ ;
  24: end if
  ( $\triangleright$ )Adaptive State Estimation
  25: if  $k \geq 1$  do
  26:  $\mathcal{J}_{f,k} = [ ]$ ; ( $\triangleright$ )empty set
  27:  $\widehat{S}_k = \text{variance}([z_0 \dots z_k])$ ; ( $\triangleright$ ) using (49)
  28: for  $i = 0$  to  $w$  do ( $\triangleright$ ) Choose  $w > 0$ 
  29:  $\eta_i = \eta_L + i(\eta_U - \eta_L)/w$ ;
  30:  $\tilde{P}_{f,k,i} = AP_{\text{da},k-1} A^T + \eta_i I_n$ ;
  31:  $\tilde{J}_{f,k,i} = \widehat{S}_k - C \tilde{P}_{f,k,i} C^T$ ;
  32: if  $\tilde{J}_{f,k,i} > 0$  do
  33:  $\mathcal{J}_{f,k} = \text{append}(\mathcal{J}_{f,k}, \tilde{J}_{f,k,i})$ ;
  34: end if
  35: end for

```

Example 6.1: Differentiation of a two-tone harmonic signal

Consider the continuous-time signal $y(t) = \sin(20t) + \sin(30t)$, where t is time in seconds. The signal $y(t)$ is sampled with sample time $T_s = 0.01$ sec. The measurements are assumed to be corrupted by noise, and thus the noisy sampled signal is given by $y_k = \sin(0.2k) + \sin(0.3k) + D_2 v_k$, where v_k is standard white noise.

Single Differentiation. For AIE/NSE, let $n_e = 12, n_f = 25, R_z = 1, R_d = 10^{-5}, R_\theta = 10^{-1} I_{25}, V_1 = 10^{-6}$, and $V_2 = 0.01$ for SNR 20 dB. For AIE/SSE, the parameters are the same as those of AIE/NSE, except that $V_{1,k}$ is adapted, where $\eta_L = 10^{-6}$

Algorithm 1 Adaptive Input Estimation/Adaptive State Estimation (AIE/ASE) (continued)

```

36:   if  $\mathcal{J}_{f,k}$  is non-empty do
37:      $\hat{J}_{f,k} = (\min \mathcal{J}_{f,k} + \max \mathcal{J}_{f,k})/2$ ;
38:      $V_{1,\text{adapt},k} = \arg \min_{\eta I_n} |J_{f,k}(\eta I_n) - \hat{J}_{f,k}|$ ;
39:      $V_{2,\text{adapt},k} = J_{f,k}(V_{1,\text{adapt},k})$ ;
40:   else do
41:      $V_{1,\text{adapt},k} = \arg \min_{\eta I_n} |J_{f,k}(\eta I_n)|$ ;
42:      $V_{2,\text{adapt},k} = 0$ ;
43:   end if
44: end if
(▷) Kalman Filter Data-Assimilation
45:    $K_{\text{da},k} = -P_{f,k}C^T(CP_{f,k}C^T + V_{2,\text{adapt},k})^{-1}$ ;
46:    $P_{\text{da},k} = (I_n + K_{\text{da},k}C)P_{f,k}$ ;
47:    $x_{\text{da},k} = x_{f,c,k} + K_{\text{da},k}z_k$ ;
(▷) Kalman Filter Forecast
48:    $P_{f,k+1} = AP_{\text{da},k}A^T + V_{1,\text{adapt},k}$ ;
49:    $x_{f,c,k+1} = Ax_{\text{da},k} + B\hat{d}_k$ 
50: end for

```

and $\eta_U = 10^2$ in Section 5.2. Similarly, for AIE/ASE, the parameters are the same as those of AIE/SSE except that $V_{2,k}$ is adapted as in Section 5.3.

Figure 6 compares the true first derivative with the estimates obtained from AIE/NSE, AIE/SSE, and AIE/ASE. Figure 7 shows that AIE/ASE has the best accuracy over the range of SNR. Figure 8 shows that the accuracy of AIE/ASE is close to the best accuracy of AIE/NSE.

Double Differentiation. For AIE/NSE, let $n_e = 12$, $n_f = 20$, $R_z = 1$, $R_d = 10^{-5}$, $R_\theta = 10^{-0.1}I_{25}$, $V_1 = 10^{-1}I_2$, and $V_2 = 0.0001$ for SNR 40 dB. For AIE/SSE, the parameters are the same as those of AIE/NSE, except that $V_{1,k}$ is adapted, where $\eta_L = 10^{-6}$ and $\eta_U = 1$ in Section 5.2. Similarly, for AIE/ASE, the parameters are the same as those of AIE/SSE except that $V_{2,k}$ is adapted as in Section 5.3.

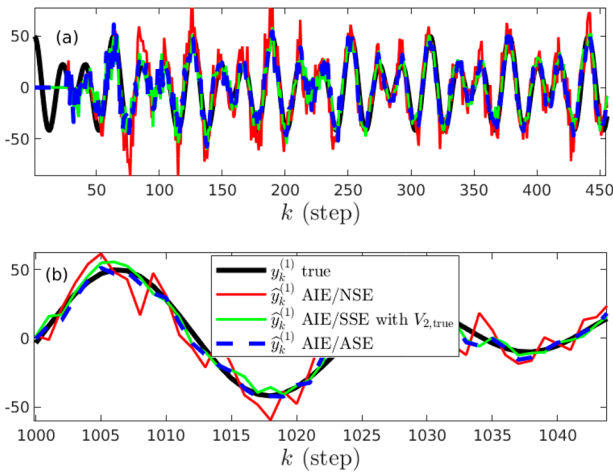


Figure 6. Example 6.1: Single differentiation of a sampled two-tone harmonic signal. (a) The numerical derivatives estimated by AIE/NSE, AIE/SSE with $V_2 = V_{2,\text{true}}$, and AIE/ASE follow the true first derivative $y^{(1)}$ after an initial transient. (b) Zoom of (a). At steady state, AIE/ASE is more accurate than both AIE/NSE and AIE/SSE with $V_2 = V_{2,\text{true}}$. The SNR is 20 dB.

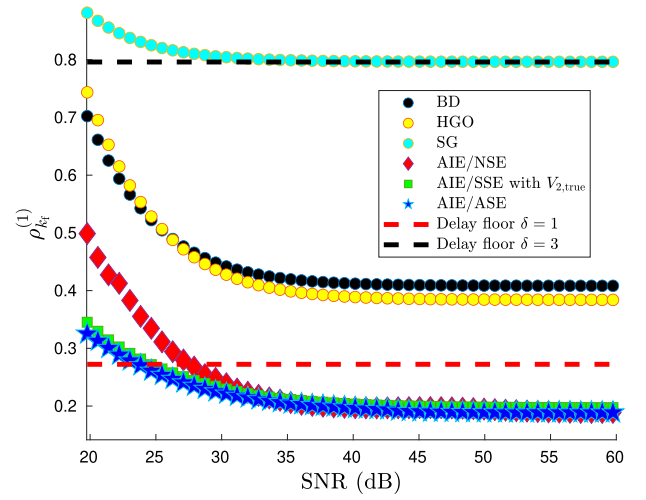


Figure 7. Example 6.1: Relative RMSE $\rho_{k_f}^{(1)}$ of the estimate of the first derivative of a two-tone harmonic signal versus SNR. AIE/ASE has the best accuracy over the range of SNR. Here $k_f = 2000$ steps.

Figure 9 compares the true second derivative with the estimates obtained from AIE/NSE, AIE/SSE with $V_2 = V_{2,\text{true}}$, and AIE/ASE. Figure 10 shows that AIE/ASE has the best accuracy over the range of SNR. Figure 11 shows that the accuracy of AIE/ASE is close to the best accuracy of AIE/NSE.

7. Application to ground-vehicle kinematics

In this section, CarSim is used to simulate a scenario in which an oncoming vehicle (the white van in Figure 12) slides over to the opposing lane. The host vehicle (the blue van) performs an evasive maneuver to avoid a collision. Relative position data along the global y-axis (shown in Figure 12) is differentiated to estimate the relative velocity and acceleration along the same axis.

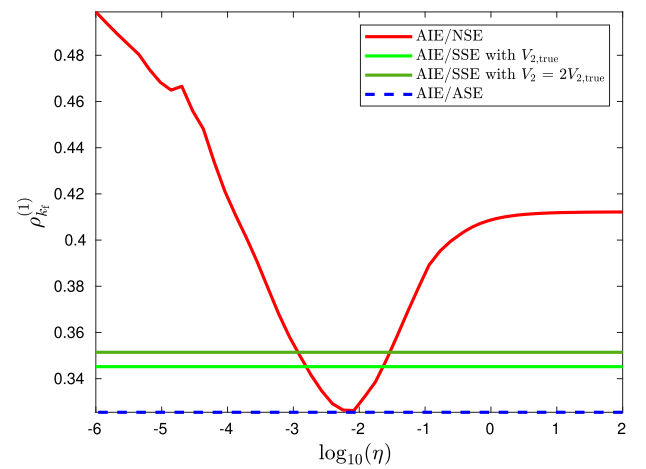


Figure 8. Example 6.1: Relative RMSE $\rho_{k_f}^{(1)}$ of the estimate of the first derivative of a two-tone harmonic signal versus η , such that $V_1 = \eta$. AIE/SSE with $V_2 = V_{2,\text{true}}$ is more accurate than AIE/SSE with $V_2 = 2V_{2,\text{true}}$, which shows the effect of V_2 on accuracy. The accuracy of AIE/ASE is close to the best accuracy of AIE/NSE. The SNR is 20 dB, and $k_f = 2000$ steps.

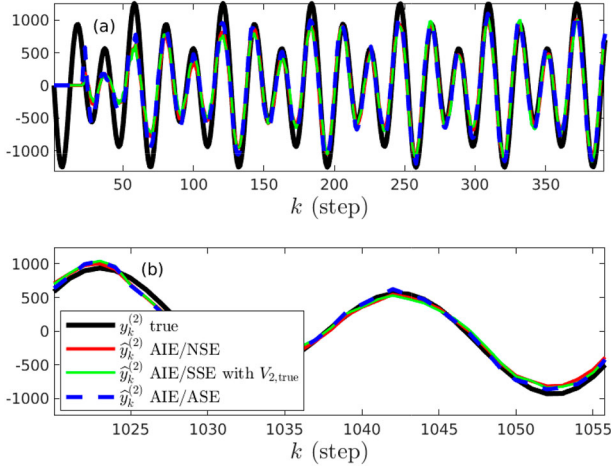


Figure 9. Example 6.1: Double differentiation of a sampled two-tone harmonic signal. (a) The numerical derivatives estimated by AIE/NSE, AIE/SSE with $V_2 = V_{2,\text{true}}$, and AIE/ASE follow the true second derivative $y^{(2)}$ after an initial transient. (b) Zoom of (a). At steady state, AIE/ASE is more accurate than AIE/SSE with $V_2 = V_{2,\text{true}}$ and AIE/NSE. The SNR is 40 dB.

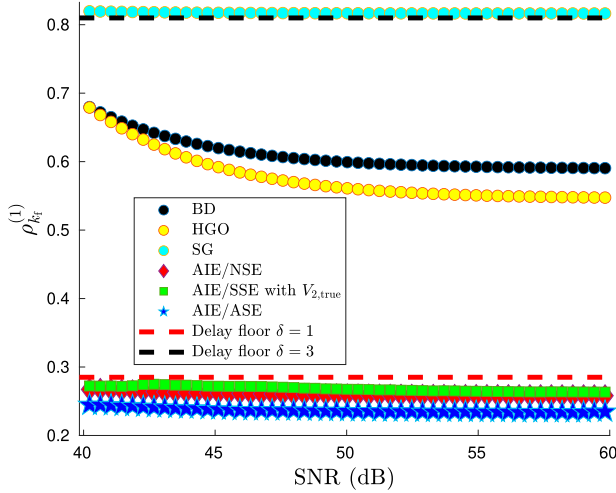


Figure 10. Example 6.1: Relative RMSE $\rho_{k_f}^{(2)}$ of the estimate of the second derivative of a two-tone harmonic signal versus SNR. AIE/ASE has the best accuracy over the range of SNR. Here $k_f = 2000$ steps.

Figure 13 shows the relative position trajectory of the vehicles on the x - y plane.

Example 7.1: Differentiation of CarSim position data.

Discrete-time position data generated by CarSim is corrupted with discrete-time, zero-mean, Gaussian white noise whose variance is chosen to vary the SNR.

Single Differentiation

For AIE/NSE, let $n_e = 25$, $n_f = 50$, $R_z = 1$, $R_d = 10^{-6}$, $R_\theta = 10^{-0.1}I_{51}$, $V_1 = 10^{-5}$, and $V_2 = 0.0049$ for SNR 40 dB. For AIE/SSE, the parameters are the same as those of AIE/NSE, except that $V_{1,k}$ is adapted, where $\eta_L = 10^{-6}$ and $\eta_U = 10^{-2}$ in Section 5.2. Similarly, for AIE/ASE, the parameters are the same as those of AIE/SSE except that $V_{2,k}$ is adapted as in Section 5.3. Figure 14 compares the true first derivative with the estimates obtained from AIE/NSE, AIE/SSE with $V_2 = V_{2,\text{true}}$, and AIE/ASE. Figure 15 shows that the accuracy of AIE/ASE is close to the best accuracy of AIE/NSE.

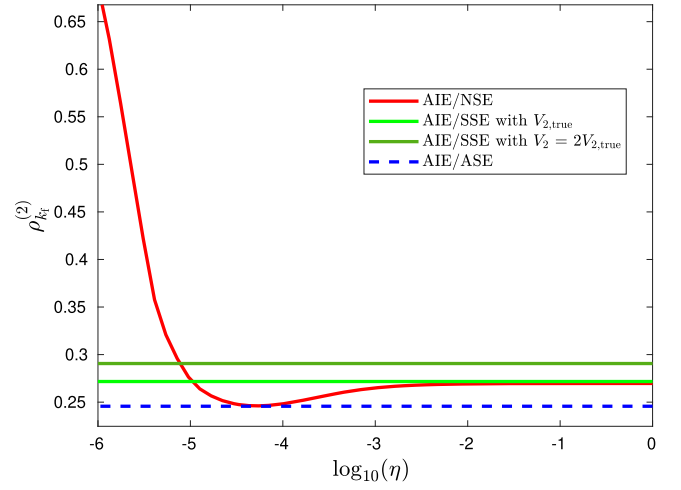


Figure 11. Example 6.1: Relative RMSE $\rho_{k_f}^{(2)}$ of the estimate of the second derivative of a two-tone harmonic signal versus η , such that $V_1 = \eta V_2$. AIE/SSE with $V_2 = V_{2,\text{true}}$ is more accurate than AIE/SSE with $V_2 = 2V_{2,\text{true}}$, which shows the effect of V_2 on accuracy. The accuracy of AIE/ASE is close to the best accuracy of AIE/NSE. The SNR is 40 dB, and $k_f = 2000$ steps.



Figure 12. Collision-avoidance scenario in CarSim. In this scenario, the oncoming vehicle (the white van) enters the opposite lane, and the host vehicle (the blue van) performs an evasive maneuver to avoid a collision.

Double Differentiation

For AIE/NSE, Let $n_e = 25$, $n_f = 21$, $R_z = 1$, $R_d = 10^{-5}$, $R_\theta = 10^{-8}I_{51}$, $V_1 = 10^{-3}I_2$, and $V_2 = 0.0049$ for SNR 40 dB. For AIE/SSE, the parameters are the same as those of AIE/NSE, except that $V_{1,k}$ is adapted, where $\eta_L = 10^{-3}$ and $\eta_U = 1$ in Section 5.2. Similarly, for AIE/ASE, the parameters are the same as those of AIE/SSE except that $V_{2,k}$ is adapted as in Section 5.3.

Figure 16 compares the true second derivative with the estimates obtained from AIE/NSE, AIE/SSE with $V_2 = V_{2,\text{true}}$, and AIE/ASE. Figure 17 shows that the accuracy of AIE/ASE is close to the best accuracy of AIE/NSE.

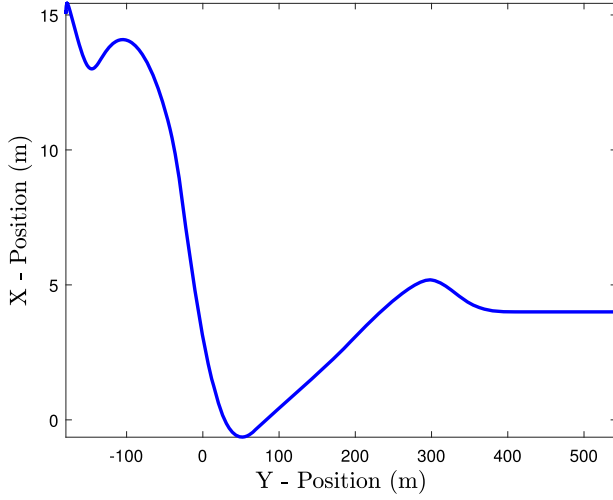


Figure 13. Collision-avoidance scenario in CarSim. Relative position trajectory of the host and the target vehicles on x - y plane.

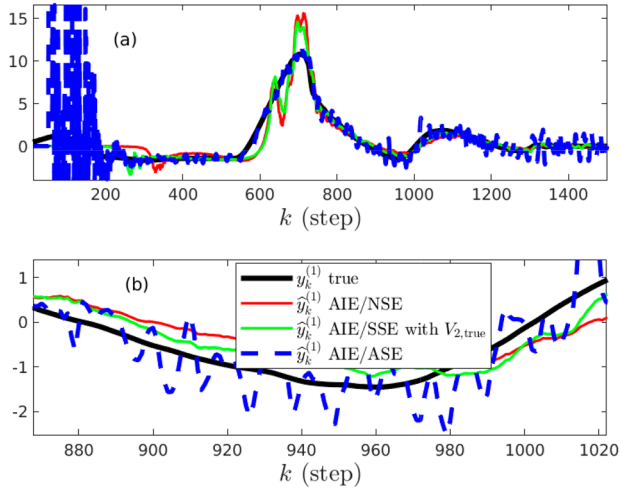


Figure 14. Example 7.1: Single differentiation of CarSim data. (a) The numerical derivatives estimated by AIE/NSE, AIE/SSE with $V_2 = V_{2,true}$, and AIE/ASE follow the true first derivative $y^{(1)}$ after an initial transient of 200 steps. (b) Zoom of (a). At steady state, AIE/ASE is more accurate than both AIE/NSE and AIE/SSE with $V_2 = V_{2,true}$. The SNR is 40 dB.

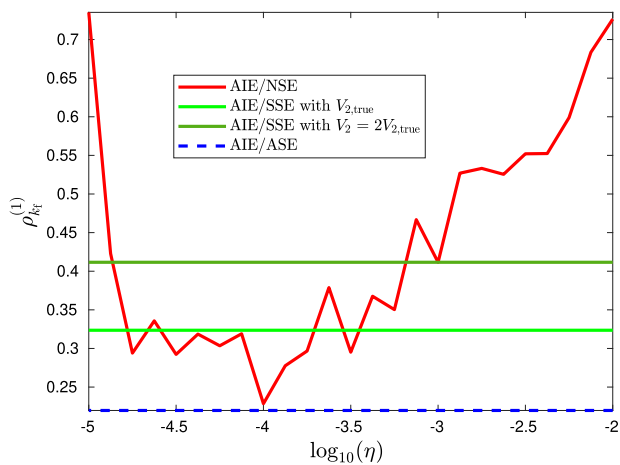


Figure 15. Example 7.1: Relative RMSE $\rho_{k_f}^{(1)}$ of the estimate of the first derivative of CarSim data versus η , such that $V_1 = \eta$. AIE/SSE with $V_2 = V_{2,true}$ is more accurate than AIE/SSE with $V_2 = 2V_{2,true}$, which shows the effect of V_2 on accuracy. The accuracy of AIE/ASE is close to the best accuracy of AIE/NSE. The SNR is 40 dB, and $k_f = 1500$ steps.

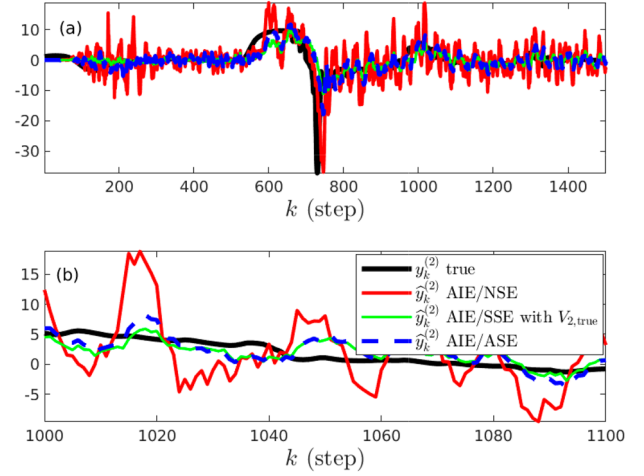


Figure 16. Example 7.1: Double differentiation of CarSim data. (a) The numerical derivatives estimated by AIE/NSE, AIE/SSE with $V_2 = V_{2,true}$, and AIE/ASE follow the true first derivative $y^{(2)}$ after an initial transient. (b) Zoom of (a). At steady state, AIE/ASE is more accurate than both AIE/NSE and AIE/SSE with $V_2 = V_{2,true}$. The SNR is 40 dB.

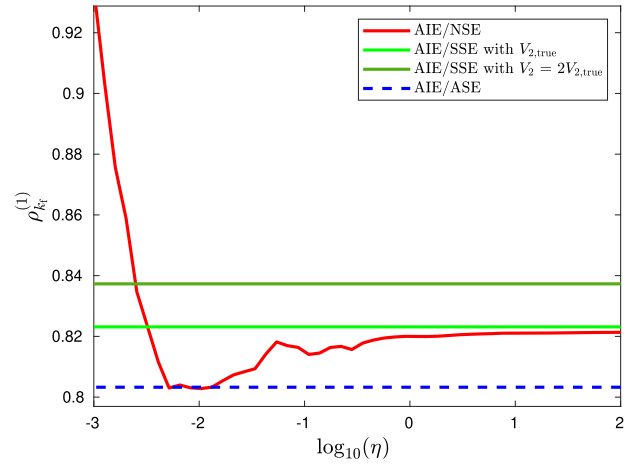


Figure 17. Example 7.1: Relative RMSE $\rho_{k_f}^{(2)}$ of the estimate of the second derivative of CarSim data versus η , such that $V_1 = \eta$. AIE/SSE with $V_2 = V_{2,true}$ is more accurate than AIE/SSE with $V_2 = 2V_{2,true}$, which shows the effect of V_2 on accuracy. The accuracy of AIE/ASE is close to the best accuracy of AIE/NSE. The SNR is 40 dB, and $k_f = 1500$ steps.

8. Conclusions

This paper presented the adaptive input and state estimation algorithm AIE/ASE for causal numerical differentiation. AIE/ASE uses the Kalman-filter residual to adapt the input-estimation subsystem and an empirical estimate of the estimation error to adapt the input-estimation and sensor-noise covariances. For dual-tone harmonic signals with various levels of sensor noise, the accuracy of AIE/ASE was compared to several conventional numerical differentiation methods. Finally, AIE/ASE was applied to simulated vehicle position data generated by CarSim.

Future work will focus on the following extensions. The minimisation of (54) was performed by using a gridding procedure; more efficient optimisation is possible.

Furthermore, it is of interest to compare the accuracy of AIE/ASE to the adaptive sliding mode differentiator in Alwi and Edwards (2013). Finally, in practice, the spectrum of

the measured signal and sensor noise may change abruptly. In these cases, it may be advantageous to replace the RLS update (41), (42) with RLS that uses variable-rate forgetting in Bruce et al. (2020) and Mohseni and Bernstein (2022).

Disclosure statement

No potential conflict of interest was reported by the author(s).

Funding

This research was supported by Ford Motor Company and NSF grant CMMI 2031333.

ORCID

Shashank Verma  <http://orcid.org/0000-0001-7673-4738>

Sneha Sanjeevini  <http://orcid.org/0000-0002-6501-9752>

E. Dogan Sumer  <http://orcid.org/0000-0002-0461-6115>

Dennis S. Bernstein  <http://orcid.org/0000-0003-0399-3039>

References

- Ahn, S., Choi, U. J., & Ramm, A. G. (2006, February). A scheme for stable numerical differentiation. *Journal of Computational and Applied Mathematics*, 186(2), 325–334. <https://doi.org/10.1016/j.cam.2005.02.002>
- Alenezi, B., Zhang, M., Hui, S., & Zak, S. H. (2021). Simultaneous estimation of the state, unknown input, and output disturbance in discrete-time linear systems. *IEEE Transactions on Automatic Control*, 66(12), 6115–6122. <https://doi.org/10.1109/TAC.2021.3061993>
- Almagbile, A., Wang, J., & Ding, W. (2010, June). Evaluating the performances of adaptive Kalman filter methods in GPS/INS integration. *Journal of Global Positioning Systems*, 9, 33–40. <https://doi.org/10.5081/jgps>
- Alwi, H., & Edwards, C. (2013). An adaptive sliding mode differentiator for actuator oscillatory failure case reconstruction. *Automatica*, 49(2), 642–651. <https://doi.org/10.1016/j.automatica.2012.11.042>
- Ansari, A., & Bernstein, D. S. (2019). Input estimation for nonminimum-phase systems with application to acceleration estimation for a maneuvering vehicle. *IEEE Transactions on Control Systems Technology*, 27(4), 1596–1607. <https://doi.org/10.1109/TCST.87>
- Astrom, K., & Hagglund, T. (2006). *Advanced PID control*. ISA.
- Bogler, P. (1987). Tracking a maneuvering target using input estimation. *IEEE Transactions on Aerospace and Electronic Systems*, AES-23(3), 298–310. <https://doi.org/10.1109/TAES.1987.310826>
- Bruce, A., Goel, A., & Bernstein, D. S. (2020). Convergence and consistency of recursive least squares with variable-rate forgetting. *Automatica*, 119, Article 109052. <https://doi.org/10.1016/j.automatica.2020.109052>
- Cullum, J. (1971). Numerical differentiation and regularization. *SIAM Journal on Numerical Analysis*, 8, 254–265. <https://doi.org/10.1137/0708026>
- Dabroom, A. M., & Khalil, H. K. (1999). Discrete-time implementation of high-gain observers for numerical differentiation. *International Journal of Control*, 72(17), 1523–1537. <https://doi.org/10.1080/002071799220029>
- Davis, P. J., & Rabinowitz, P. (1984). *Methods of numerical integration* (2nd ed.). Dover.
- Da-yan Liu, O. G., & Perruquetti, W. (2011). Differentiation by integration with Jacobi polynomials. *Journal of Computational and Applied Mathematics*, 235(9), 3015–3032. <https://doi.org/10.1016/j.cam.2010.12.023>
- Fang, H., Shi, Y., & Yi, J. (2011). On stable simultaneous input and state estimation for discrete-time linear systems. *Journal of Adaptive Control and Signal Processing*, 25(8), 671–686. <https://doi.org/10.1002/ac.s.v25.8>
- Farrell, J. A. (2008). *Aided navigation: GPS with high rate sensors*. McGraw-Hill.
- Gilljins, S., & De Moor, B. (2007). Unbiased minimum-variance input and state estimation for linear discrete-time systems. *Automatica*, 43(1), 111–116. <https://doi.org/10.1016/j.automatica.2006.08.002>
- Grewel, M. S., Andrews, A. P., & Bartone, C. G. (2020). *Global navigation satellite systems, inertial navigation, and integration* (4th ed.). Wiley.
- Haimovich, H., Seeber, R., Aldana-López, R., & Gómez-Gutiérrez, D. (2022). Differentiator for noisy sampled signals with best worst-Case accuracy. *IEEE Control Systems Letters*, 6, 938–943. <https://doi.org/10.1109/LCSYS.2021.3087542>
- Hamming, R. W. (1973). *Numerical methods of scientists and engineers* (2nd ed.). Dover.
- Hide, C., Moore, T., & Smith, M. (2003, January). Adaptive Kalman filtering for low-cost INS/GPS. *The Journal of Navigation*, 56, 143–152. <https://doi.org/10.1017/S0373463302002151>
- Hsieh, C. S. (2017). Unbiased minimum-variance input and state estimation for systems with unknown inputs: A system reformation approach. *Automatica*, 84, 236–240. <https://doi.org/10.1016/j.automatica.2017.06.037>
- Ibrir, S., & Diop, S. (2004). A numerical procedure for filtering and efficient high-Order signal differentiation. *International Journal of Applied Mathematics and Computer Science*, 14(2), 201–208.
- Islam, S. A. U., & Bernstein, D. S. (2019). Recursive least squares for real-time implementation. *IEEE Control Systems Magazine*, 39(3), 82–85. <https://doi.org/10.1109/MCS.5488303>
- Jauberteau, F., & Jauberteau, J. (2009). Numerical differentiation with noisy signal. *Applied Mathematics and Computation*, 215, 2283–2297. <https://doi.org/10.1016/j.amc.2009.08.042>
- Jia, Z., Balasuriya, A., & Challa, S. (2008). Autonomous vehicles navigation with visual target tracking: Technical approaches. *Algorithms*, 1(2), 153–182. <https://doi.org/10.3390/a1020153>
- Kalata, P. R. (1984). The tracking index: A generalized parameter for α - β and α - β - γ target trackers. *IEEE Transactions on Aerospace and Electronic Systems*, AES-20(2), 174–182. <https://doi.org/10.1109/TAES.1984.310438>
- Khaloozadeh, H., & Karsaz, A. (2009). Modified input estimation technique for tracking manoeuvring targets. *IET Radar, Sonar & Navigation*, 3(1), 30–41. <https://doi.org/10.1049/iet-rsn:20080028>
- Knowles, I., & Renka, R. J. (2014). Methods for numerical differentiation of noisy data. *Electronic Journal of Differential Equations*, 2014, 235–246.
- Lee, H., & Tahk, M. J. (1999). Generalized input-estimation technique for tracking maneuvering targets. *IEEE Transactions on Aerospace and Electronic Systems*, 35(4), 1388–1402. <https://doi.org/10.1109/7.805455>
- Levant, A. (1998). Robust exact differentiation via sliding mode technique. *Automatica*, 34(3), 379–384. [https://doi.org/10.1016/S0005-1098\(97\)00209-4](https://doi.org/10.1016/S0005-1098(97)00209-4)
- Levant, A. (2003). Higher-order sliding modes, differentiation and output-feedback control. *International Journal of Control*, 76(9-10), 924–941. <https://doi.org/10.1080/0020717031000099029>
- Li, P., Pin, G., Fedele, G., & Parisini, T. (2018). Non-asymptotic numerical differentiation: A kernel-based approach. *International Journal of Control*, 91(9), 2090–2099. <https://doi.org/10.1080/00207179.2018.1478130>
- Listmann, K. D., & Zhao, Z. (2013). *A comparison of methods for higher-order numerical differentiation* [Paper presentation]. European Control Conference (ECC), Zurich, Switzerland.
- López-Caamal, F., & Moreno, J. A. (2019). Generalised multivariable super-twisting algorithm. *International Journal of Robust and Nonlinear Control*, 29(3), 634–660. <https://doi.org/10.1002/rnc.v29.3>
- Mboup, M., Join, C., & Fliess, M. (2009). Numerical differentiation with annihilators in noisy environment. *Numerical Algorithms*, 50, 439–467. <https://doi.org/10.1007/s11075-008-9236-1>
- Mehra, R. K. (1972). Approaches to adaptive filtering. *IEEE Transactions on Automatic Control*, 17, 693–698. <https://doi.org/10.1109/TAC.1972.1100100>
- Moghe, R., Zanetti, R., & Akella, M. R. (2019). Adaptive Kalman filter for detectable linear time-invariant systems. *Journal of Guidance, Control, and Dynamics*, 42(10), 2197–2205. <https://doi.org/10.2514/1.G004359>

- Mohamed, A. H., & Schwarz, K. P. (1999). Adaptive Kalman filtering for INS/GPS. *Journal of Geodesy*, 73, 193–203. <https://doi.org/10.1007/s001900050236>
- Mohseni, N., & Bernstein, D. S. (2022). *Recursive Least Squares with Variable-Rate Forgetting Based on the F-Test* [Paper presentation]. American Control Conference (ACC), Atlanta, GA, USA.
- Mojallizadeh, M. R., Brogliato, B., & Acary, V. (2021). Discrete-time differentiators: Design and comparative analysis. *International Journal of Robust and Nonlinear Control*, 31(16), 7679–7723. <https://doi.org/10.1002/rnc.v31.16>
- Mook, D. J., & Junkins, J. L. (1988). Minimum model error estimation for poorly modeled dynamic systems. *Journal of Guidance, Control, and Dynamics*, 11(3), 256–261. <https://doi.org/10.2514/3.20302>
- Naderi, E., & Khorasani, K. (2019). Unbiased inversion-based fault estimation of systems with non-minimum phase fault-to-output dynamics. *IET Control Theory & Applications*, 13(11), 1629–1638. <https://doi.org/10.1049/cth2.v13.11>
- Nieuwstadt, M. V., Rathinam, M., & Murray, R. M. (1998). Differential flatness and absolute equivalence of nonlinear control systems. *SIAM Journal on Control and Optimization*, 36(4), 1225–1239. <https://doi.org/10.1137/S0363012995274027>
- Orjuela, R., Marx, B., Ragot, J., & Maquin, D. (2009). On the simultaneous state and unknown input estimation of complex systems via a multiple model strategy. *IET Control Theory & Applications*, 3(7), 877–890. <https://doi.org/10.1049/iet-cta.2008.0148>
- Polyakov, A., Efimov, D., & Perruquetti, W. (2014). *Homogeneous differentiator design using implicit Lyapunov Function method* [Paper presentation]. European Control Conference (ECC).
- Rana, M. M., Halim, N., Rahamna, M. M., & Abdelhadi, A. (2020). *Position and Velocity Estimations of 2D-Moving Object Using Kalman Filter: Literature Review* [Paper presentation]. 22nd International Conference on Advanced Communication Technology (ICACT).
- Reichhartinger, M., & Spurgeon, S. (2018). An arbitrary-order differentiator design paradigm with adaptive gains. *International Journal of Control*, 91(9), 2028–2042. <https://doi.org/10.1080/00207179.2018.1429671>
- Savitzky, A., & Golay, M. J. (1964). Smoothing and differentiation of data by simplified least squares procedures. *Analytical Chemistry*, 36(8), 1627–1639. <https://doi.org/10.1021/ac60214a047>
- Schafer, R. W. (2011). What is a Savitzky-Golay filter? *IEEE Signal Processing Magazine*, 28(4), 111–117. <https://doi.org/10.1109/MSP.2011.941097>
- Shi, Y., Han, C., & Liang, Y. (2009). *Adaptive UKF for target tracking with unknown process noise statistics* [Paper presentation]. 12th International Conference on Information Fusion, Seattle, WA, USA.
- Staggs, J. E. J. (2005). Savitzky–Golay smoothing and numerical differentiation of cone calorimeter mass data. *Fire Safety Journal*, 40(6), 493–505. <https://doi.org/10.1016/j.firesaf.2005.05.002>
- Stickel, J. (2010). Data smoothing and numerical differentiation by a regularization method. *Computers & Chemical Engineering*, 34, 467–475. <https://doi.org/10.1016/j.compchemeng.2009.10.007>
- Van Breugel, F., Kutz, J. N., & Brunton, B. W. (2020). Numerical differentiation of noisy data: A unifying multi-objective optimization framework. *IEEE Access*, 8, 196865–196877. <https://doi.org/10.1109/Access.6287639>
- Verma, S., Sanjeevini, S., Sumer, E. D., Girard, A., & Bernstein, D. S. (2022). *On the Accuracy of Numerical Differentiation Using High-Gain Observers and Adaptive Input Estimation* [Paper presentation]. American Control Conference (ACC), Atlanta, GA, USA.
- Vilanova, R., & Visioli, A. (2012). *PID control in the third millennium: Lessons learned and new approaches*. Springer.
- Yaesh, I., & Shaked, U. (2008). Simplified adaptive estimation. *Systems & Control Letters*, 57, 49–55. <https://doi.org/10.1016/j.sysconle.2007.06.015>
- Yong, S. Z., Zhu, M., & Frazzoli, E. (2016). A unified filter for simultaneous input and state estimation of linear discrete-time stochastic systems. *Automatica*, 63, 321–329. <https://doi.org/10.1016/j.automatica.2015.10.040>
- Zhang, L., Sidoti, D., Bienkowski, A., Pattipati, K. R., Bar-Shalom, Y., & D. L. Kleinman (2020). On the identification of noise covariances and adaptive Kalman filtering: A new look at a 50 year-old problem. *IEEE Access*, 8, 59362–59388. <https://doi.org/10.1109/Access.6287639>